Available online at BCREC Website: https://bcrec.id

Bulletin of Chemical Reaction Engineering & Catalysis, 15 (1) 2020, xxx-xxx

Research Article

Effect of Process Parameters on the Photocatalytic Degradation of Phenol in Oilfield Produced Wastewater using ZnO/Fe_2O_3 Nanocomposites

Omer Al Haiqi[1,*], Abdurahman Hamid Nour[1], Rushdi Bargaa[1], Bamidele Victor Ayodele[2]

[1]Faculty of Chemical and Process Engineering Technology, College of Engineering Technology, Universiti Malaysia Pahang, Lebuhraya Tun Razak, Gambang-Kuantan 26300, Malaysia.
[2]Institute of Energy Policy and Research, Universiti Tenaga Nasional, Jalan IKRAM-UNITEN, 4300 Kajang, Malaysia.

Received: 8th October 2019; Revised: 5th November 2019; Accepted: 5th November 2019; Available online: 30th March 2020; Published regularly: April 2020

Abstract

The upstream processing of crude oil is often associated with the presence of phenolic compounds when not properly treated could result in adverse effects on human health. The objective of the study was to investigate the effect of process parameters on the photocatalytic degradation of phenol. The ZnO/Fe_2O_3 nanocomposite photocatalyst was prepared by sol-gel method and characterized using various instrument techniques. The characterized ZnO/Fe_2O_3 nanocomposite displayed suitable physicochemical properties for the photocatalytic reaction. The ZnO/Fe_2O_3 nanocomposite was employed for the phenol degradation in a cylindrical batch reactor under solar radiation. The photocatalytic runs show that calcination temperature of the ZnO/Fe_2O_3 nanocomposite, catalyst loading, initial phenol concentration and pH of the wastewater significantly influence the photocatalytic degradation of phenol. After 180 min of solar radiation, the highest phenol degradation of 92.7% was obtained using the ZnO/Fe_2O_3 photocatalyst calcined at 400 °C. This study has demonstrated that phenol degradation is significantly influenced by parameters such as calcination temperature of the ZnO/Fe_2O_3 nanocomposite, catalyst loading, initial phenol concentration and pH of the wastewater resulting in highest phenol degradation using the ZnO/Fe_2O_3 nanocomposite calcined at 400 °C, initial phenol concentration of 0.5 mg/L, catalyst loading of 3 mg/L and pH of 3.

Keywords: Degradation; Photocatalyst; Phenol; Wastewater; ZnO/Fe_2O_3 nanocomposites

How to Cite: Al Haiqi, O., Nour, A.H., Bargaa, R., Ayodele, B.V. (2020). Effect of Process Parameters on the Photocatalytic Degradation of Phenol in Oilfield Produced Wastewater using ZnO/Fe_2O_3 Nanocomposites. *Bulletin of Chemical Reaction Engineering & Catalysis*, 15(1), xxx-xxx (doi:10.9767/bcrec.15.1.6068.xxx-xxx)

Permalink/DOI: https://doi.org/10.9767/bcrec.15.1.6068.xxx-xxx

1. Introduction

The processing of crude oil in onshore facilities is often accompanied by the use of a huge amount of water [1]. This produced wastewater usually contains some toxic pollutants that if not properly treated before disposal could threaten human health [2]. Besides, in the arid region such as the middle east where there is a high shortage of water, effective treatment of the produced wastewater to meet the stipulated standard can make it be re-used for agricultural purposes [3]. One of such toxic chemicals that need to be properly removed from the produced wastewater is phenol [4]. The United States Environmental Protection Agency (EPA) has

* Corresponding Author.
Email: omaralhaigi@gmail.com (O. Al Haiqi)

branded phenol as one of the priority pollutants in wastewater that needs urgent attention due to its high risk to human health even at very low concentrations [5]. Hence, strict limits regarding the concentration of phenol allowed in wastewater have been set by various international regulatory agencies, such as EPA [6,7]. Based on the EPA standard, the concentration of phenol in treated wastewater must not exceed 1 part per billion (ppb) [5]. Exposure of wastewater containing phenol concentration between 9-15 mg/L could lead to serious health problems [8].

Techniques such as biodegradation, physical separation, and advanced oxidation process have been employed for the treatment of wastewater targeting the removal of recalcitrant pollutants [9-11]. Amongst these techniques used for the treatment of wastewater containing phenolic compounds, advance oxidation process has been reported as an efficient strategy. Moradi *et al*. [12] employed iron-doped TiO_2 for the degradation of phenol and reported 57% phenol removal from the wastewater. In a similar study by Zhang *et al*. [13], Co-Pd/$BiVO_4$ photocatalyst was employed for the degradation of phenol under visible light irradiation. The degradation of 90% phenol was attained after 180 min of visible light irradiation. The variation in the amount of phenol degraded in Moradi *et al*. [12] and Zhang *et al*. [13] can be attributed to the variation in the physicochemical properties of the photocatalysts and the differences in the process parameters. Recently, the use of nanocomposite photocatalysts, such as: AgBr/BiOBr/graphene, BiOCl-TiO_2, ZnO/Nd-doped BiOBr, and Ag-ZnO for the photocatalytic degradation of phenol under visible light, have been reported [14-17]. These studies revealed that phenol was effectively degraded from the wastewater using the nanocomposite photocatalysts. In the present study ZnO/Fe_2O_3 nanocomposite synthesized by sol-gel was employed for the degradation of phenol in produce wastewater obtained from an onshore oil wastewater treatment facility. The effect of ZnO/Fe_2O_3 nanocomposite calcination temperature, catalyst loading, initial phenol concentration and the pH of the wastewater on the phenol degradation was investigated.

2. Materials and Methods

The sample of the produced water used for the experimentation was obtained from the produced wastewater treatment plant, Masila, Yemen. The water sample was stored in an air-tight dark bottle and refrigerated before using for the experimental runs. The initial concentration of phenol was determined from the water sample.

The ZnO/Fe_2O_3 nanocomposite photocatalyst was prepared using precursors materials, such as: zinc nitrate hexa-hydrate ($Zn(NO_3)_2.6H_2O$, 99.999% trace metal bases, Sigma-Aldrich), iron (III) nitrate nonahydrate ($Fe(NO_3)_3.9H_2O$, 99.999% trace metal bases, Sigma-Aldrich), ethanol (90% by volume), ethylene glycol (99.8% purity), hydrochloric acid (99.8%m purity), and citric acid (99.5% purity). Sol-gel method standards for the synthesis of the ZnO/Fe_2O_3 photocatalyst [18]. To prepare the photocatalyst, $Zn(NO_3)_2.6H_2O$ and $Fe(NO_3)_3.9H_2O$ were dissolved in a beaker containing 100 ml ethanol in a molar ratio of 1:3 and stirred for 30 min using a magnetic stirrer. A 3 mol of citric acid and 50 ml ethanol was prepared separately and added to the colloidal gel-like salt-solution. The entire mixture was subsequently stirred continuously at 60 ºC on a hot plate for 60 min. This enables the completion of the hydrolysis and condensation with the addition of NH_3 and HCl occasionally to regulate the pH of the gel. Thereafter the obtained gel was allowed to dry in an oven at 80 ºC for 40 min to form a xerogel which was calcined 400 ºC for 3 h to obtain the ZnO/Fe_2O_3 nanocomposite photocatalyst. The crystallinity, the textural properties, the morphology and the photo-properties of the ZnO/Fe_2O_3 photocatalysts were examined by X-ray Diffractometer (XRD), Field Emission Scanning Electron Microscope (FESEM), N_2 physisorption analysis and UV/Vis spectrophotometer.

2.1 Phenol Degradation

The as-prepared ZnO/Fe_2O_3 nanocomposite was tested for photo-degradation of phenol in the produced wastewater under direct solar radiation. The effects of parameters such as ZnO/Fe_2O_3 calcination, phenol initial concentration, photocatalyst loading, and pH of the produced wastewater on phenol degradation was examined. A cylindrical batch reactor (non-concentrating type slurry reactor) was employed for the photodegradation experimental runs. For each of the experimental runs, 100 mL of the produced wastewater was used together with the specified amount of ZnO/Fe_2O_3 nanocomposite ranges from 0.5-3 mg/L was added to the oil field produced water and continuously stirred under dark for 60 minutes. The produced water containing the photocatalyst was placed under direct solar radiation to commence the photodegradation re-

action. About 0.5 to 1.0 mL of the aliquot was collected at 15-minutes interval after the commencement of the experimental runs. The aliquot was centrifuged and filtered. The concentration of the phenol left in the treated produce water was measured using High-performance Liquid Chromatography (486-WFMA HPLC). The extent of photocatalytic degradation of the phenol in the produced wastewater was calculated using Equation (1):

$$DE\,\% = \frac{C_0 - C}{C_0} \times 100 \quad (1)$$

where C_0 is the initial concentration at t = 0 and C is the concentration of toxic compounds at different intervals of irradiation time, t = t_{min}.

3. Results and Discussion

3.1 Characterization of the ZnO/Fe_2O_3 Nanocatalyst

Figure 1 depicts the XRD pattern of the ZnO/Fe_2O_3 nanocomposite photocatalyst. The XRD pattern shows reflective peaks well indexed at 2-theta values of 29.94°, 31.89°, 34.32°, 35.98°, 44.28°, 48.78°, 56.65°, 58.32°, 62.22°, and 67.78° to the hexagonal structure of $Fe_{0.1}O_1Zn_{0.9}$ nanocomposite with International Centre for Diffraction Data (ICDD) no of 98-008-9727 [19]. The XRD pattern did not capture ZnO and Fe_2O_3 which implies that the oxides were aggregated to form $Fe_{2.02}O_4Zn_{0.96}$ nanocomposite [20].

The N_2 physisorption analysis of the ZnO/Fe_2O_3 nanocomposites showing the adsorption-desorption isotherm is depicted in Figure 2. The adsorption isotherm displayed a typical Type IV adsorption isotherm with the H3-hysteresis loop in accordance with the International Union of Pure and Applied Chemistry (IUPAC) classifications [21,22]. This is an indication of weakly adsorption of liquid N_2 onto the surface of the ZnO/Fe_2O_3 nanocomposites with evidence of capillary condensation occurring in photocatalyst mesopore [23]. The Brunauer-Emmett-Teller (BET) specific surface area and the Berrett-Joyner-Halenda

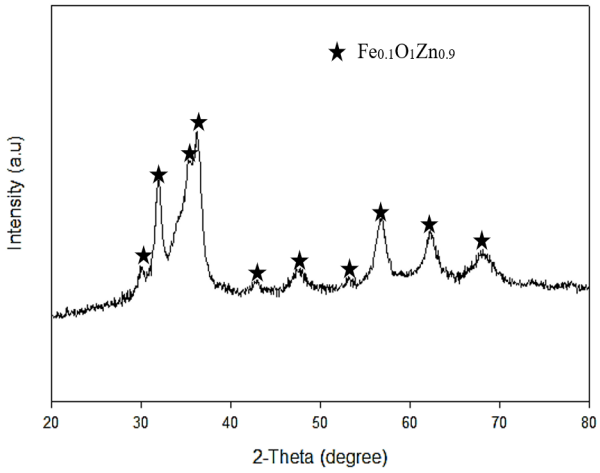

Figure 1. XRD pattern of the ZnO/Fe_2O_3 nanocomposite.

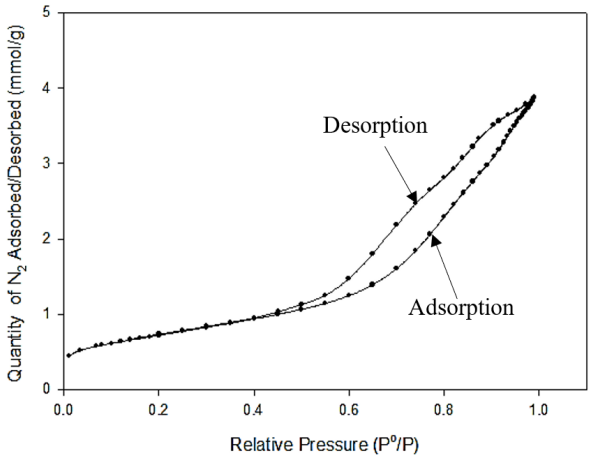

Figure 2. Adsorption-Desorption isotherm of the ZnO/Fe_2O_3 nanocomposite.

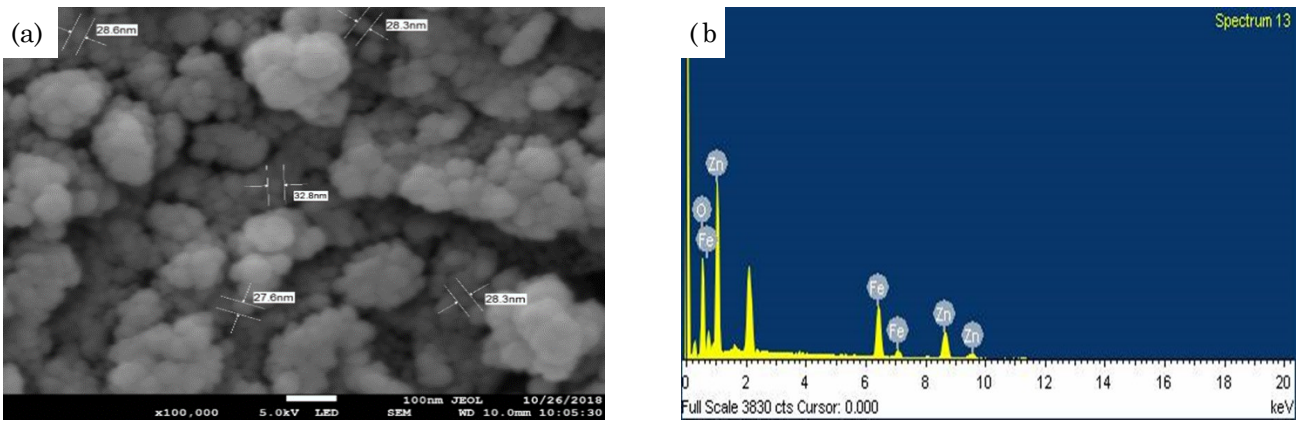

Figure 3. (a) The FESEM images and (b) EDX micrographs of the ZnO/Fe_2O_3 nanocomposite.

(BJH) pore volume of the ZnO/Fe_2O_3 nanocomposites are estimated as 57.64 m^2/g and 0.137 cm^3/g, respectively. The pore diameter of the ZnO/Fe_2O_3 photocatalyst was obtained as 9.34 nm which further confirms the mesoporous nature of the ZnO/Fe_2O_3 nanocomposites since a mesoporous material has an average pore diameter greater than 2 nm [24].

Figure 3 depicted the FESEM image and the EDX micrograph showing the morphology and the elemental composition of the ZnO/Fe_2O_3 photocatalyst. The FESEM image revealed a spherical cluster of ZnO/Fe_2O_3 nanocomposites as shown in Figure 3 (a). The average particle size of the nanocomposite taken at five different points was calculated as 29.12 nm. An evidence of agglomeration of the spherical nanocomposites can be observed which might have occurred during the calcination process. The detail elemental composition of the ZnO/Fe_2O_3 nanocomposites is represented in Figure 3 (b). The different elements such as Zn, O, and Fe which make up the photocatalyst are well represented by the EDX micrograph which further establishes the suitability of the sol-gel method used for preparing the ZnO/Fe_2O_3 photocatalyst [25].

Figure 4 shows the UV-vis absorption spectra of the ZnO/Fe_2O_3 photocatalyst. It can be seen that the ZnO/ Fe_2O_3 photocatalyst exhibited absorption peaks in both the ultra-violet and the visible regions as indicated by the wavelength range. This revealed the suitability of the ZnO/Fe_2O_3 nanocomposites as photocatalyst that can be employed for degradation of phenol using enormous potential solar energy resources in the visible light region.

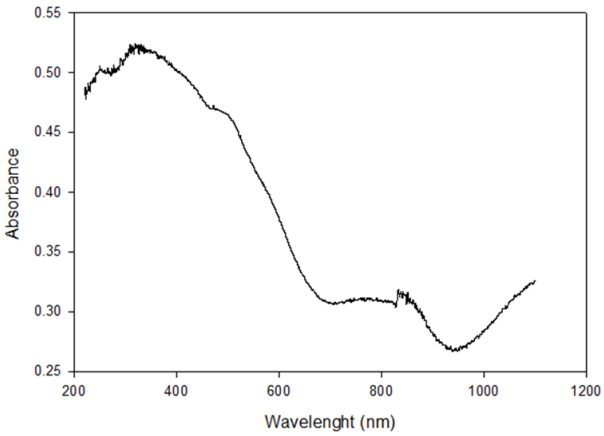

Figure 4. UV-vis absorption spectra for the ZnO/Fe_2O_3 nanocomposite.

3.2 Effect of Process Parameters on the Photodegradation of Phenol

3.2.1 Photocatalyst calcination temperature

The effect of varying calcination temperature on the photocatalytic activities of the ZnO/Fe_2O_3 photocatalyst using 1-2 mg/L of the photocatalysts as well as 0.5 and 3 mg/L of the phenol concentration are depicted in Figure 5 and 6. In Figure 5, it can be seen that the degradation of the phenol in the produced wastewater increases with an increase in the irradiation time for each of the ZnO/Fe_2O_3 photocatalysts calcined at 400 °C, 500 °C, and 600 °C using 1 mg/L of the photocatalyst and 0.5 mg/L of the phenol concentration. However, at irradiation time less than 120 min, the degradation of phenol was higher with ZnO/Fe_2O_3 photocatalysts calcined at 500 °C and 600 °C

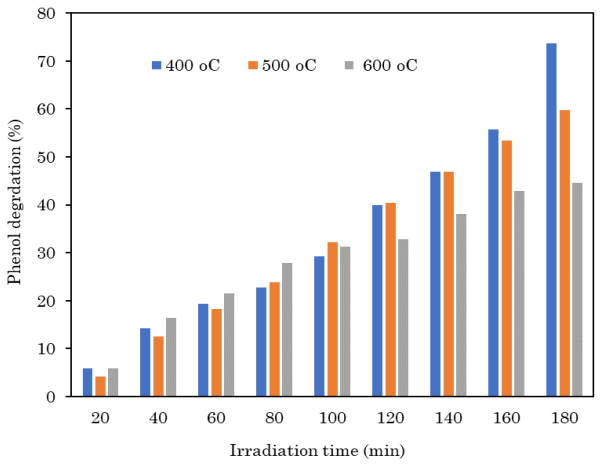

Figure 5. Degradation of phenol for ZnO/Fe_2O_3 calcined at 400 °C, 500 °C, and 600 °C (Photocatalyst amount: 1 mg/L, phenol concentration of 0.5 mg/L).

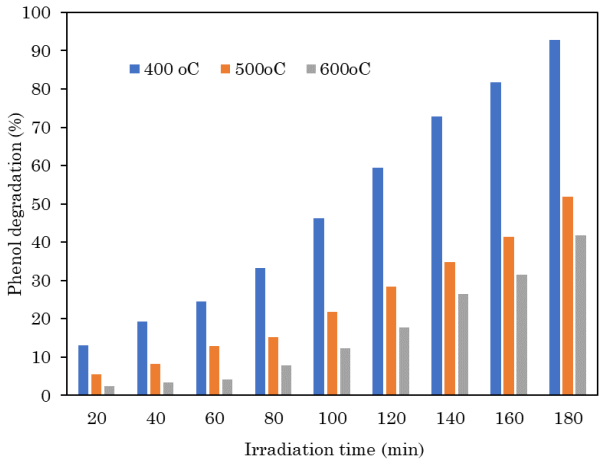

Figure 6. Degradation of phenol for calcined at 400 °C, 500 °C, and 600 °C (Photocatalyst amount: 2 mg/L, phenol concentration of 3 mg/L).

compared to the ZnO/Fe_2O_3 photocatalysts calcined at 400 ºC. This trend could be attributed to non-steady uptake of the phenol probably due to its low concentration. As time progresses, there was a steady adsorption of the phenol from the wastewater. This observation was only peculiar to low concentration of phenol. After 180 mins photodegradation of the phenol under solar radiation, 73.6%, 59.8%, and 44.6% of the phenol have been degraded by the ZnO/Fe_2O_3 photocatalyst calcined at 400 ºC, 500 ºC, and 600 ºC, respectively. This implies that the photodegradation of the phenol is strongly dependent on the calcination temperature of the photocatalyst. Interestingly, the highest phenol degradation from the produced wastewater was obtained using the ZnO/Fe_2O_3 photocatalyst calcined at 400 ºC. This agrees with the work of Kangle *et al.* [26] who reported the effect of calcination of the photocatalytic activity of TiO_2 used for degrading surface fluorine. Obviously, an increase in calcination temperature probably has effects on the pores of the photocatalysts indicated by the cumulative pore volume of 0.137 cm^3/g, 0.127 cm^3/g, 0.078 cm^3/g for calcination temperature of 400 ºC, 500 ºC, and 600 ºC, respectively. The pores of the photocatalysts are responsible for the adsorption of the phenol prior to photodegradation reaction. Moreover, the increase, in calcination temperature could also lead to decrease in the BET surface areas (57.65 m^2/g, 20.72 m^2/g, and 7.67 m^2/g for calcination temperature of 400 ºC, 500 ºC, and 600 ºC, respectively) which could be responsible for the decrease in photocatalytic activity as reported by Xiao and Ouyang [27]. Also, the effect of varying calcination temperature on the photocatalytic activity using a higher photocatalyst amount of 2 mg/L and phenol concentration of the 3 mg/L is depicted in Figure 6. Similarly, the activity of the photocatalyst decreases with increases in the calcination temperature. After 180 min irradiation time, the 92.7%, 41.4%, and 41.7% of the phenol in the produced wastewater have been degraded using the ZnO/Fe_2O_3 photocatalyst calcined at 400 ºC, 500 ºC, 600 ºC, respectively. With increase in the phenol concentration and the amount of photocatalyst, the amount of phenol degraded in the produced wastewater also increases using ZnO/Fe_2O_3 photocatalyst calcined at 400 ºC. These results suggest that attaining high phenol degradation requires the use of ZnO/Fe_2O_3 photocatalyst calcined at a temperature around 400 ºC. Comparing Figure 5 and 6 on the bases of the amount of photocatalyst used and the concentration of the phe-

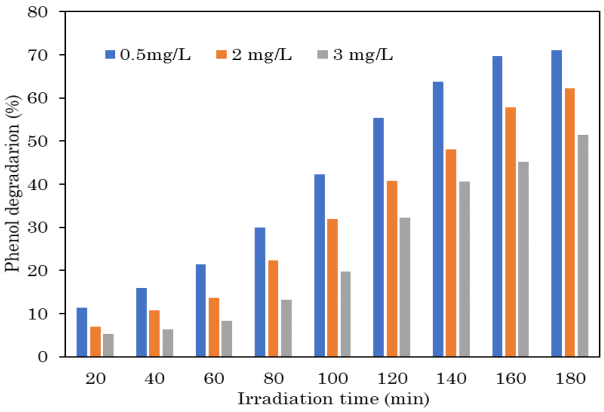

Figure 7. Degradation of phenol at different initial phenol concentration (ZnO/Fe_2O_3 calcined at 400 ºC and photocatalyst loading of 2 mg/L and pH = 3).

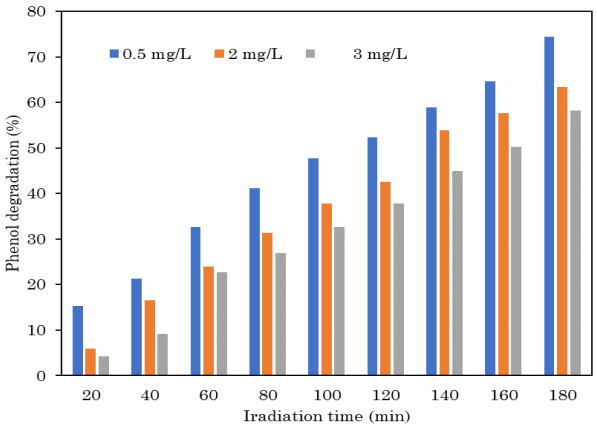

Figure 8. Degradation of phenol at different phenol initial concentration (ZnO/Fe_2O_3 calcined at 500 ºC, photocatalyst loading of 2 mg/L, pH = 3).

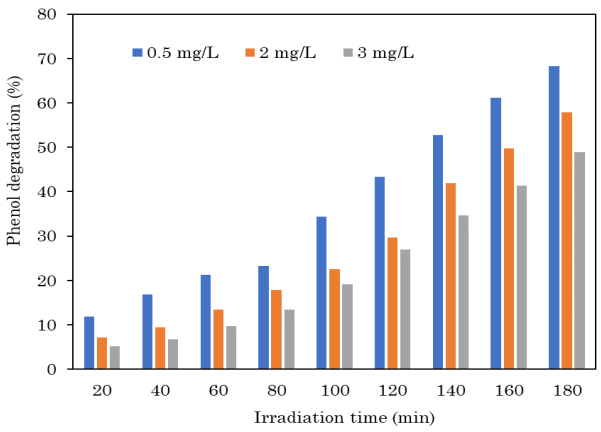

Figure 9. Degradation of phenol under at different phenol initial concentration (ZnO/Fe_2O_3 calcined at 600 ºC, photocatalyst load of 2 mg/L, pH = 3).

nol, it can be seen that a more steady degradation of the phenol was observed using 1 mg/L of the ZnO/Fe_2O_3 photocatalysts calcined at 400 °C, 500 °C, 600 °C and phenol concentration of 0.5 mg/L compared to using 2 mg/L of ZnO/Fe_2O_3 photocatalyst calcined at 400 °C, 500 °C, 600 °C for 3 mg/L of phenol concentration. Nevertheless, the highest phenol degradation was recorded using 2 mg/L of the ZnO/Fe_2O_3 photocatalyst calcined at 400 °C and phenol concentration of 3 mg/L.

3.2.2 Effect of initial phenol concentration

The effect of initial phenol concentration on the degradation of phenol using ZnO/Fe_2O_3 photocatalyst calcined at 400 °C, 500 °C, and 600 °C are shown in Figures 7-9, respectively. In Figure 7, 2 mg/L of the ZnO/Fe_2O_3 photocatalyst calcined at 400 °C was employed for the photodegradation of the phenol in the produced water. It can be seen that the photodegradation of the phenol decreases with an increase in the initial phenol concentration. After 180 min of solar radiation, 71.1%, 62.3%, and 51.5% of phenol were degraded from the produced water at 0.5, 2, and 3 mg/L initial phenol concentration, respectively. Also, in Figure 8, 2 mg/L of the ZnO/Fe_2O_3 photocatalyst calcined at 500 °C was employed for the photodegradation of the phenol in the produced water. The photodegradation of the phenol varies with the initial phenol concentration in the produced water. After 180 min, 74.5%, 63.4%, and 58.2% of the phenol present in produced water have been degraded from the produced water with the initial phenol concentration of at 0.5, 2, and 3 mg/L, respectively. Similar, Figure 9 shows the variation of the amount of phenol degraded using different initial phenol concentration. Phenol degradation was 68.3%, 57.8%, and 48.9% after 180 mins using at 0.5, 2, and 3 mg/L initial phenol concentration. Muhammad *et al.* [28] reported that a higher phenol concentration often leads to low phenol degradation efficiency which is in agreement with trend obtained in this study. The present study is consistent with that of Paul *et al.* [29] who reported that g-C_3N_4 photocatalyst at various loading significantly influences the photodegradation of methylene blue in contaminated water. The presence of high concentration of phenol in the solution entails more time to attain the same removal rate as the low concentration of phenol, hence gives rise to low phenol degradation efficiency.

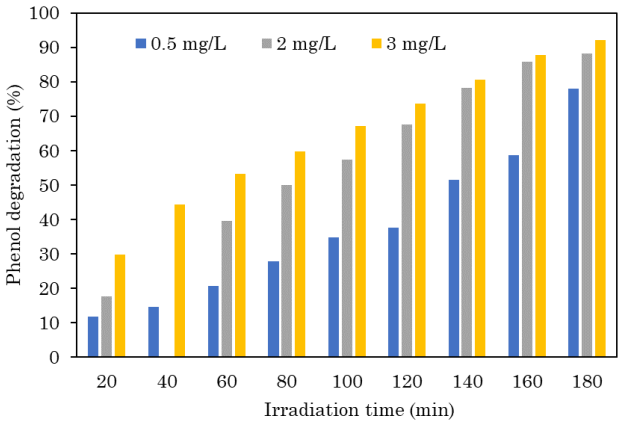

Figure 10. Degradation of phenol at varying amount of ZnO/Fe_2O_3 calcined at 400 °C (Phenol initial concentration of 3 mg/L; pH = 3).

3.2.3 Effect of photocatalyst loading

Figures 10-12 show the effect of photocatalyst loading on the phenol degradation using photocatalyst calcined at 400 °C, 500 °C, and

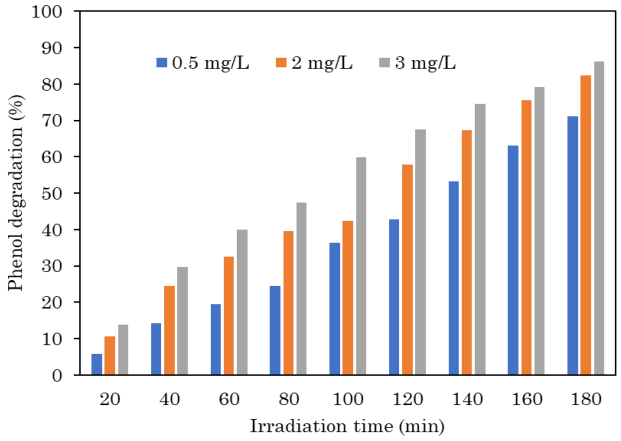

Figure 11. Degradation of phenol at varying amount of ZnO/Fe_2O_3 calcined at 500 °C (Phenol initial concentration of 3 mg/L; pH = 3).

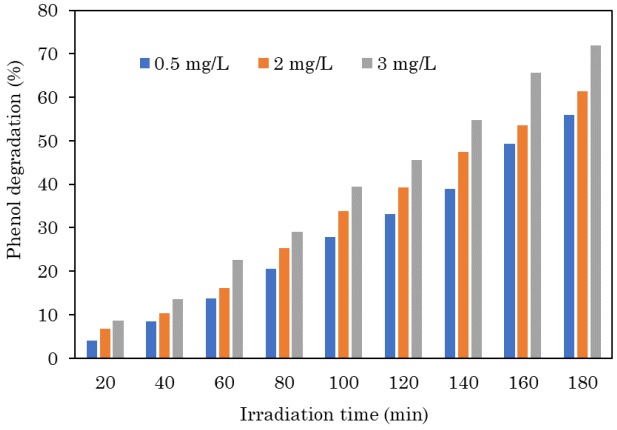

Figure 12. Degradation of phenol at varying amount of ZnO/Fe_2O_3 calcined at 600 °C (Phenol initial concentration of 3 mg/L; pH = 3).

600 ºC, respectively. The amount of the photocatalyst was varied from 0.5 to 3 mg/L. Figure 10 depicts the photodegradation of phenol at different photocatalyst loading (the photocatalyst was calcined at 400 ºC). It can be seen that the photodegradation of the phenol increases with an increase in the photocatalyst loading [30]. After 180 min, 77.9%, 88.2%, and 92.2% have been degraded from the produced water using photocatalyst loading of 0.5 mg/L, 2 mg/L, and 3 mg/L, respectively. A similar trend was observed for the photocatalyst calcined at 500 ºC used at various loading for the photodegradation reaction. The degradation of the phenol in the produced wastewater increase with the photocatalyst loading. Phenol degradation of 71.2%, 82.4%, and 86.2% were obtained for photocatalyst loading of 0.5 mg/L, 1 mg/L, and 3 mg/L, respectively after 180 min of solar radiation. Moreover, the photodegradation of phenol using the photocatalyst calcined at 600 ºC followed the same trend with the amount phenol degraded in the produced wastewater increases with increase in the photocatalyst loading. 55.9%, 61.4%, and 71.9% of the phenol degraded using 0.5 mg/L, 2 mg/L, and 3 mg/L of the photocatalyst, respectively.

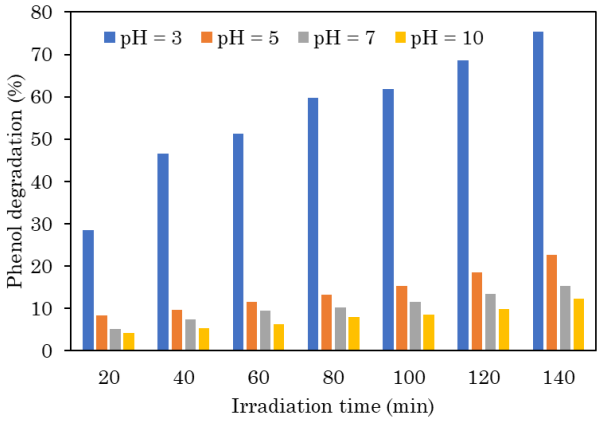

Figure 13. Degradation of phenol at varying pH (ZnO/Fe_2O_3 calcined at 400 ºC) (photocatalyst load 3 mg/L and phenol initial concentration 3 mg/L).

3.2.4 Effect of pH

The effect of pH on the photocatalytic degradation of phenol using ZnO/Fe_2O_3 photocatalyst calcined at a temperature range of 400-600 ºC is depicted in Figures 13-15. Studies have shown that photocatalytic degradation of recalcitrant pollutants is often affected by the pH of the solution [29]. Figure 10 depicts the effect of pH on the photodegradation of phenol in produce water using ZnO/Fe_2O_3 calcined at 400 ºC. The initial pH solution of the produced wastewater was set at 3, 5, 7, and 10 which covers acidic, neutral and alkaline solution. It is obvious that the amount of phenol degraded from the produced wastewater decreases with increase in the pH of the water. After 180 min of solar radiation, 75.3%, 22.6%, 15.2%, and 12.3% of phenol was degraded from the produced wastewater with pH of 3, 5, 7, and 10 respectively. This implies that the formation of radicals needed to adsorb on the surface of the photocatalyst is facilitated in the acidic medium as displayed in this study. A similar observation was observed using ZnO/Fe_2O_3 photocatalyst calcined at 500 ºC for the degradation of phenol in the produced wastewater depicted in Figure 14. At 180 min, 69.5%, 23.1%, 16.3%

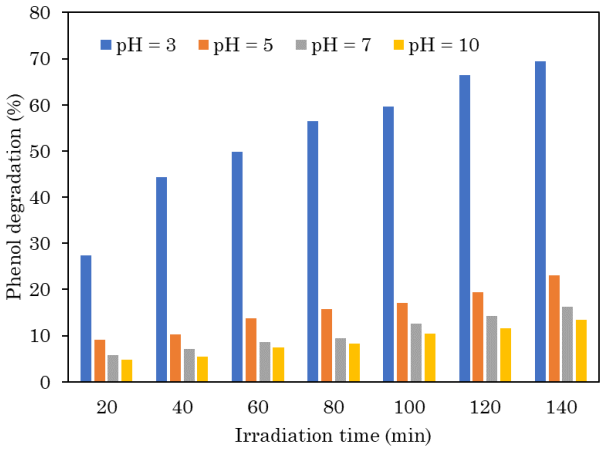

Figure 14. Degradation of phenol at varying pH (ZnO/Fe_2O_3 calcined at 500 ºC) (photocatalyst load: 3 mg/L and phenol initial concentration 3 mg/L).

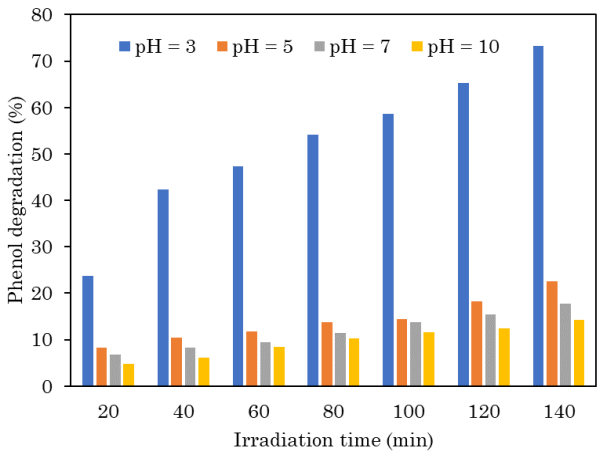

Figure 15. Degradation of phenol at varying pH (ZnO/Fe_2O_3 calcined at 600 ºC, catalyst loading: 3 mg/L and phenol initial concentration: 3 mg/L).

and 13.5% phenol have been degraded from the produced wastewater with pH of 3, 5, 7, and 10 respectively. For the ZnO/Fe_2O_3 calcined at 600 °C, similar trend was also observed for the degradation of phenol in the produced water at different pH values. In the produced wastewater with pH of 3, 5, 7 and 10, the photocatalytic process resulted in the degradation of 73.3%, 22.6%, 17.7%, and 14.2%, respectively.

4. Conclusion

In this study, the effects of parameters such as ZnO/Fe_2O_3 nanocomposite calcination temperature, catalyst loading, initial phenol concentration and pH of the wastewater on the phenol degradation have been investigated. For each of the parameters considered, the amount of phenol degradation was found to increase with the irradiation time. Hence, the three parameters were found to significantly influence the amount of phenol degraded from the wastewater. The amount of phenol degradation was found to increase with an increase in the photocatalyst loading but decrease with increase in calcination temperature and pH of the wastewater. The maximum phenol degradation was attained using ZnO/Fe_2O_3 nanocomposite photocatalyst calcined at 400 °C, initial phenol concentration of 0.5mg/L, catalyst loading of 3 mg/L and pH of 3. The combination of these parameters can further be optimized for efficient photodegradation of the phenol from the produced wastewater.

Acknowledgment

....???? Especially Funder of Research....

References

[1] Gonzalez, R., Scarlat, N. (2020). Overview of the Water Requirements for Energy Production in Africa, in: V. Naddeo, M. Balakrishnan, K.-H. Choo (Eds.). *Front. Frontiers in Water-Energy-Nexus - Nature-Based Solutions, Advanced Technologies and Best Practices for Environmental Sustainability*. Cham, Switzerland. Springer International Publishing 417–420. DOI: 10.1007/978-3-030-13068-8_104

[2] Liang, Y., Ning, Y., Liao, L., Yuan, B. (2018). Special Focus on Produced Water in Oil and Gas Fields: Origin, Management, and Reinjection Practice, in: B. Yuan, D.A. Wood (Eds.), *Formation Damage During Improved Oil Recovery*. Houston, Texas. Gulf Professional Publishing. 515–586. DOI: 10.1016/B978-0-12-813782-6.00014-2

[3] Zehtabiyan-Rezaie, N., Alvandifar, N., Saffaraval, F., Makkiabadi, M., Rahmati, N., Saffar-Avval, M. (2019). A solar-powered solution for water shortage problem in arid and semi-arid regions in coastal countries. *Sustainable Energy Technologies and Assessments*, 35, 1–11. DOI: 10.1016/j.seta.2019.05.015

[4] Liu, F. (year???). Polyaniline/MWCNT Nanocomposite as Sensor for Electroanalytical Determination of Phenol in Oil Field Wastewater. *International Journal of Electrochemical Science*, 14, 9122–9131. DOI: 10.20965/2019.09.79

[5] Environmental Protection Agency (2002). Toxicological Review for Phenol. http://www.epa.gov/iris.

[6] World Health Organization (1994). Phenol Health and safety Guide No. 88. https://apps.who.int/iris/handle/10665/39958

[7] Environmental Protection Agency (2000). Phenol. https://www.epa.gov/sites/production/files/2016-09/documents/phenol.pdf.

[8] Bruce, R.M., Santodonato, J., Neal, M.W. (1987). Summary review of the health effects associated with Phenol. *Toxicology Industrial. Health*, 3(4), 535–568. DOI: 10.1177/074823378700300407

[9] Villegas, L.G.C., Mashhadi, N., Chen, M., Mukherjee, D., Taylor, K.E., Biswas, N.A. (year????). Short Review of Techniques for Phenol Removal from Wastewater. *Current Pollution Reports*, 2(3), 157–167. DOI:10.1007/s40726-016-0035-3.

[10] Ke, Q., Zhang, Y., Wu, X., Su, X., Wang, Y., Lin, H., Mei, R., Zhang, Y., Hashmi, M.Z. Chen, C., Chen, J. (2018). Sustainable biodegradation of phenol by immobilized Bacillus sp. SAS19 with porous carbonaceous gels as carriers. *Journal of Environmental Management*, 222, 185–189. DOI: 10.1016/j.jenvman.2018.05.061.

[11] Fernandes, A., Makoś, P., Khan, J.A., Boczkaj, G. (2019). Pilot scale degradation study of 16 selected volatile organic compounds by hydroxyl and sulfate radical based advanced oxidation processes. *Journal of Cleaner. Production,* 208, 54–64. DOI: 10.1016/j.jclepro.2018.10.081.

[12] Moradi, V., Ahmed, F., Jun, M.B.G., Blackburn, A., Herring, R.A. (2019). Acid-treated Fe-doped TiO_2 as a high performance photocatalyst used for degradation of phenol under visible light irradiation. *Journal of Environmental Science*, 83, 183–194. DOI: 10.1016/j.jes.2019.04.002.

[13] Zhang, Y., Gao, B., Lu, L., Yue, Q., Wang, Q., Jia, Y. (2010). Treatment of produced water from polymer fl ooding in oil production by the combined method of hydrolysis acidification-dynamic membrane bioreactor – coagulation process. *Journal of Petroleum Science and Engineering*, 74, 14–19. DOI: 10.1016/j.petrol.2010.08.001.

[14] Vaiano, V., Matarangolo, M., Murcia, J.J., Rojas, H., Navío, J.A., Hidalgo, M.C. (2018). Enhanced photocatalytic removal of phenol from aqueous solutions using ZnO modified with Ag. *Applied Catalysis B: Environmental,* 225, 197–206. DOI:10.1016/j.apcatb.2017.11.075.

[15] Sin, J-.C., Lim, C-.A., Lam, S-.M., Mohamed, A.R., Zeng, H. (2019). Facile synthesis of novel ZnO/Nd-doped BiOBr composites with boosted visible light photocatalytic degradation of phenol. *Material Letters,* 248, 20–23. DOI: 10.1016/j.matlet.2019.03.129.

[16] Singh, P., Raizada, P., Sudhaik, A., Shandilya, P., Thakur, P., Agarwal, S., Gupta, V.K. (2019). Enhanced photocatalytic activity and stability of AgBr/BiOBr/graphene heterojunction for phenol degradation under visible light, *Journal of Saudi Chemical Society*, 23, 586–599. DOI: 10.1016/j.jscs.2018.10.005.

[17] Sánchez-Rodríguez, D., Medrano, M.G.M., Remita, H., Escobar-Barrios, V. (2018) Photocatalytic properties of BiOCl-TiO_2 composites for phenol photodegradation. *Journal of Environmental Chemical Engineering*, 6, 1601–1612. DOI: 10.1016/j.jece.2018.01.061.

[18] Tao, X., Li, X., Huang, L., Wang, G., Ye, Q. (2016). Highly active Ni–Ce/TiO_2–Al_2O_3 catalysts: Influence of preparation methods. *International Journal of Hydrogen Energy*, Vol?? (issue??), page???? DOI: 10.1016/j.ijhydene.2016.03.031.

[19] Aliah, H., Syarif, D.G., Iman, R.N., Sawitri, A., Darmalaksana, W., Setiawan, A., Malik, A. Gumarang, P. (2019). Structure Analysis of Nanocomposite ZnO:Fe_2O_3 based Mineral Yarosite as Fe_2O_3 Source and its Application Probability. *Material Today Proceedings*, 13, 36–40. DOI: 10.1016/j.matpr.2019.03.183.

[20] Xie, J., Zhou, Z., Lian, Y., Hao, Y., Li, P., Wei, Y. (2015). Synthesis of α -Fe_2O_3 /ZnO composites for photocatalytic degradation of pentachlorophenol under UV–vis light irradiation. *Ceramics International*, 41, 2622–2625. DOI: 10.1016/j.ceramint.2014.10.043.

[21] Sing, K.S.W., Williams, R.T. (2004). Physisorption Hysteresis Loops and the Characterization of Nanoporous Materials. *Adsorption Science and Technology*, 22, 773–782. DOI: 10.1260/0263617053499032.

[22] Donohue, M., Aranovich, G., (1998). Classification of Gibbs adsorption isotherms. *Advances in Colloid and Interface Science,* 76–77, 137–152. DOI: 10.1016/S0001-8686(98)00044-X.

[23] Groen, J.C., Peffer, L.A., Pérez-Ramirez, J. (2003). Pore size determination in modified micro- and mesoporous materials. Pitfalls and limitations in gas adsorption data analysis, *Microporous Mesoporous Materials*, 60, 1–17. DOI: 10.1016/S1387-1811(03)00339-1.

[24] Huang, B., Bartholomew, C.H., Woodfield, B.F. (2014). Improved calculations of pore size distribution for relatively large, irregular slit-shaped mesopore structure. *Microporous Mesoporous Materials*, 184, 112–121. DOI: 10.1016/j.micromeso.2013.10.008.

[25] Benrabaa, R., Löfberg, A., Guerrero Caballero, J., Bordes-Richard, E., Rubbens, A., Vannier, R-N., Boukhlouf, H., Barama, A. (2015). Sol–gel synthesis and characterization of silica supported nickel ferrite catalysts for dry reforming of methane. *Catalysis Communication*, 58, 127–131. DOI: 10.1016/j.catcom.2014.09.019.

[26] Lv, K., Xiang, Q., Yu, J. (2011). Effect of calcination temperature on morphology and photocatalytic activity of anatase TiO_2 nanosheets with exposed {001} facets. *Applied Catalysis B: Environmental*, 104, 275–281. DOI: 10.1016/j.apcatb.2011.03.019.

[27] Xiao, Q., Ouyang, L. (2009). Photocatalytic activity and hydroxyl radical formation of carbon-doped TiO_2 nanocrystalline: Effect of calcination temperature. *Chemical Engineering Journal*, 148, 248–253. DOI: 10.1016/j.cej.2008.08.024.

[28] Muhammad, S., Saputra, E., Sun, H., Izidoro, J.D.C., Fungaro, D.A., Ang, H.M., Tadé, M.O., Wang, S. (2012). Coal fly ash supported Co_3O_4 catalysts for phenol degradation using peroxymonosulfate. *RSC Advances*, 2, 5645–5650. DOI: 10.1039/c2ra20346d.

[29] Paul, T., Das, D., Das, B.K., Sarkar, S., Maiti, S., Chattopadhyay, K.K. (2019). $CsPbBrCl_2$/g-C_3N_4 type II heterojunction as efficient visible range photocatalyst. *Journal of Hazardous Materials*, 380, 120855. DOI: 10.1016/j.jhazmat.2019.120855.

[30] Ayodele, B.V., Khan, M.R., Nooruddin, S.S., Cheng, C.K. (2017). Modelling and optimization of syngas production by methane dry reforming over samarium oxide supported cobalt catalyst: response surface methodology and artificial neural networks approach. *Clean Technologies and Environmental Policy*, 19(4), 1181-1193.